Journal of Thermal Biology 72 (2018) 127–136

Contents lists available at ScienceDirect

Journal of Thermal Biology

journal homepage: www.elsevier.com/locate/jtherbio

Estimation of the optimum number and location of nanoparticle injections and the specific loss power for ideal hyperthermia

Mostafa Pasandi Boroon[a], Mohammad-Bagher Ayani[a,*], Sajad Razavi Bazaz[b]

[a] Department of Mechanical Engineering, Ferdowsi University of Mashhad, Mashhad, Iran
[b] Department of Life Science Engineering, Faculty of New Sciences and Technologies, University of Tehran, Tehran, Iran

ARTICLE INFO

Keywords:
Magnetic fluid hyperthermia
Inverse method
Magnetic nanoparticles
Uniform temperature elevation
Specific loss power

ABSTRACT

Hyperthermia is one of the most appealing methods of cancer treatment in which the temperature of tumor is elevated to reach a desired temperature. One of the methods of increasing tissue temperature is injection of nanoparticle fluids to tumor and applying alternative magnetic field, which is called magnetic nanoparticle hyperthermia method. The total number of injection points, as well as the their location within a tissue play a significant role in this method. Furthermore, the power of heating of a magnetic material per gram or specific loss power (SLP) is another important factor which needs to be investigated. As the uniform temperature of 43 °C is effective enough for a tumor regression in certain specific tissues, the inverse method is applied to find out both the number of injection points and their location. Furthermore, the effective amount of heat generated by nanoparticles is investigated by this technique. Two-dimensional cancerous brain tissue was considered, zero gradients on boundary conditions were assumed, and diffusion equation and Pennes equation, which is regarded as energy equation, were solved, respectively. Conjugate gradient technique as a one way of inverse methods is applied, and unknowns are investigated. The results illustrate that three-point injection with the best injection sites cannot induce a uniform temperate distribution of 43 °C, and although four-point injection can create a uniform temperature elevation, the amount of it cannot reach the 43 °C. Finally, the optimum locations of five-point injection which are ((0.80,3.24), (0.80,0.84), (2.00,2.00), (3.20,3.24), (3.32,0.84)) (all dimensions are in mm) in the studied domain with special loss power of 420 W/g, all of which are obtained after 36 iterations, demonstrate that these conditions can meet the requirements of the magnetic fluid hyperthermia and can be considered for the future usage of researchers and investigators.

1. Introduction

Thermal therapy or hyperthermia is a method for cancer therapy in which a specific tissue is subjected to the prescribed high temperature which leads to destruction of cancer cells with minimum damage to other tissues (Habash et al., 2006). In general, the main target of hyperthermia is increasing the temperature of particular cells. Magnetic fluid hyperthermia (MFH) is one of the most effective types of hyperthermia in which tumor is heated by internal heat sources. Magnetic particles in the form of thermoseeds or magnetic nanoparticles are injected into a tumor, and then, exposed to an alternating magnetic field with proper amplitude and frequency. Due to hysteresis and viscous losses, these magnetic particles ultimately increase the temperature of cancerous tissue (Johannsen et al., 2004). In temperature above 42 °C, the tumor turns out to the phenomenon known as acidosis, which decreases PH of a cancerous cell and eventually results in the tumor regression (Jalali et al., 2014; Katz and Willner, 2004).

In recent years, many materials have been examined in order to use as thermoseeds in various kinds of hyperthermia (Atsumi et al., 2006). One of the initial studies on the particle injection was carried out by Jordan et al. (1999). They used two different ferrofluids in their study which are magnetite particles with aminosilan type shell and with dextran type shell. The first one had largely positive surface charges and the second one had a neutral to negative surface charge. The temperature of about 45 °C in the tissue was their achievement. Cobalt-palladium thermoseeds, Self-regulating thermoseeds type, used by Deger et al. (2003) to examine the effect of interstitial hyperthermia combined with radiation on prostate cancer. There weren't any major side effect during this treatment and the temperature of intra-prostate was reported about 44 °C. The results showed that the combination of hyperthermia with conformal radiotherapy may be another curative treatment option for the prostate cancer. Park et al., 2002, in a report, studied the duplex stainless steel thermoseeds and their heating features, especially their effect on rabbit liver in the induction of

* Corresponding author.
E-mail address: mbayani@um.ac.ir (M.-B. Ayani).

https://doi.org/10.1016/j.jtherbio.2018.01.010
Received 27 July 2017; Received in revised form 20 January 2018; Accepted 22 January 2018
Available online 31 January 2018
0306-4565/

Nomenclature

C	nanoparticles concentration
C_p	Specific heat capacity
d	direction of the descent
D	diffusion coefficient
D^*	effective diffusion coefficient
J	sensitivity matrix
k	thermal conductivity
P	vector of unknown parameters
q_m	cellular metabolism
q_g	heat produced by nanoparticles
Q	injection rate
s	source term
S	objective function
T	temperature
V	injection volume
W	calculated quantities
L	characteristic length of square domain
x,y	x- and y-coordinate system
Y	desired quantities

Greek symbols

α	porosity
β	search step size
γ	conjugation coefficient
λ	tortuosity
ω_b	blood perfusion

Subscripts

b	blood

Superscripts

k	number of iterations
T	transpose of the vector

hyperthermia. Their study included both in vivo and in vitro studies with thermoseeds of two different shapes, L-shaped and I-shaped. By using magnetic induction field, they could reach the temperature about 55 °C. Therefore, these kinds of thermoseeds with magnetic induction field could be considered effective in the induction of interstitial hyperthermia.

Despite various advantages, thermoseeds have their negative implications. They should be planted in cancerous tissue by surgery. If the cancerous tissue has a complex shape, the planting of these seeds will be practically impossible and overpriced. Furthermore, using these seeds cannot cause a uniform temperature distribution (Salloum et al., 2009). Over the last four decades, there has been a sharp increase of interest in using nanoparticles in laboratory studies. Use of nanoparticles in MFH has been highly regarded by the researchers in the recent decade (Baghban and Ayani, 2017; Tartaj and Serna, 2003). The major advantages of magnetic nanoparticles in comparison with magnetic thermoseeds are high surface-to-volume ratio and different crystal structures, which increase the heat generated in the tumor. From 2001 on, numerous researchers have focused on using magnetic nanoparticles in MFH. The diffusion and its transport mechanism of brain tissue was carefully examined by Charles Nicholson. This study can be regarded as a turning point in the development of molecular diffusion within a tissue, especially brain tissue (Nicholson, 2001). Another outstanding study in this field was carried out by Brusentsov et al. (2002). They developed magnetic dextran-ferrite #363 (DF) nanoparticles for a special kind of hyperthermia in which AC magnetic field externally was applied. They also concluded that to achieve complete tumor regression, it is crucial to use both AC magnetic field and DF nanoparticles. Laurent et al. (2011) investigated MFH by Superparamagnetic nanoparticles both experimentally and numerically, and temperature of this type of nanoparticles was estimated more than other types. Golneshan and Lahonian (2011) examined numerically nanoparticle concentration in a cancerous tissue by lattice Boltzmann method, and the results were compared with analytical ones. They were able to achieve a nearly uniform distribution of nanoparticles with four-point injection in the tumor. The effect of some relative factors such as surface coating on nanoparticles were scrutinized by Liu et al. (2012). They showed that by optimization of both surface coating and particle size in nanometer, specific absorption rate (SAR) reached the highest rate. Vallejo-Fernandez and O'Grady (2013) examined the effect of the distribution of anisotropy constants on hysteresis losses for MFH applications. They analytically proved that in order to have an exact model for MFH, the effect of both particle size and thermal conductivity distribution should be considered. Deatsch and Evans (2014) contextualized studies about the effect of nanoparticle concentration on heating efficiency and showed that there was a negative relationship between magnetic relaxation time and nanoparticle concentration. Smolkova et al., 2015 in 2015 studied about iron oxide nanoparticles. Their main purpose was getting a relationship between magneto-structural properties of those nanoparticles and their heating efficiency for better performance of MFH. Moreover, in our recent research, an inverse algorithm was used to estimate the external power of source term in a multilayer skin tissue (Baghban and Ayani, 2015), and also, non-Fourier heat conduction during hyperthermia in a biolayer spherical living tissue was investigated (Mohajer et al., 2016).

Injected points of ferrofluids are important factors on the nanoparticle concentration within the tissue. As a matter of fact, the non-uniform concentration of nanoparticles cannot create a uniform temperature distribution, and it not only decreases the efficacy of MFH but also may change the shape of cancerous cells into complex ones, which are much more resistant against MFH. A quick glance at the review papers shows that no one works on the location of the injection points on the hyperthermia. To overcome the foregoing problems, in this study, the precise injection points and the necessary amount of special loss power (SLP) for the uniform temperature of 43 °C are obtained by using the inverse method. Maximum five points of injection are evaluated for a two-dimensional tissue. Overall, the inverse method should determine unknowns, including precise injection point coordinates and SLP. For reaching this purpose, first, governing equations that used in this study should be clarified, these are completely discussed in Section 2. Then in Section 3, the inverse method with all assumptions are explained. After that, the results will be discussed and the best conditions for this method will be illustrated.

2. Governing equations and geometry design

The whole human body has numerous complex tissues that are different from one place to another one. Physical properties of each tissue including conductivity, average temperature, and porosity are unique and different to each other. Therefore, a specific tissue should be considered for the inverse method. In this study, cancerous brain tissue was considered. The main aspect that should be mentioned is that the brain tissue as itself has a completely complex shape which makes it very difficult for the numerical modeling. Therefore, modeling of the brain is obtained by considering the following hypotheses:

1. Extracellular fluid is stagnant (Davson, 1993).
2. Brain tissue is regarded as a porous medium without considering

capillary network (Jain et al., 2007; Soltani and Chen, 2011).

2.1. Diffusion equation

With above hypotheses, the diffusion balance equation for brain tissue can be expressed as below (Nicholson, 2001):

$$\frac{\partial C}{\partial t} = D^*\nabla^2 C + \frac{s}{\alpha} \tag{1}$$

where C is the nanoparticle concentration, α is the porosity, s is the mass source term which is relied on the ferrofluid density and inserted on the each element of the grid. It is good to mention that the source term in Eq. (1) is a discrete parameter, and for analytical solution, a Dirac delta function in both space and time is required, but, in here, the problem solved numerically, and it is added in each element, and in other elements, its value sets as zero, and by doing so, the equation is solved. D^* is the effective diffusion coefficient, which is given as (Nicholson, 2001):

$$D^* = \frac{D}{\lambda^2} \tag{2}$$

where λ and D are the tortuosity and the mass diffusion coefficient, respectively.

2.2. Energy equation

Pennes equation (Pennes, 1948), one of the most precise models for energy conservation in living tissue, is used to calculate temperature distribution in the brain tissue:

$$\rho C_p \frac{\partial T}{\partial t} = \nabla.(k\nabla T) + \omega_b \rho_b C_{pb}(T_b - T) + q_m + q_g \tag{3}$$

where ρ is the tissue density, C_p is the specific heat capacity of tissue, k is the thermal conductivity of tissue, T is the tissue temperature, is ρ_b the blood density, C_{pb} is the specific heat capacity of blood, T_b is the blood temperature, ω_b is the blood perfusion, q_m is the cellular metabolism, and q_g is the total heat produced by nanoparticles which can be expressed as (Pennes, 1948):

$$q_g = SLP \times C \tag{4}$$

where SLP is the specific loss power of nanoparticles which is caused by an external alternating magnetic field.

2.3. Geometry design and boundary and initial conditions

The physical domain of the considered problem is displayed in Fig. 1. It concerns a cancerous brain tissue in a 2D square domain with characteristic length of L. Thermophysical and physical properties of the tissue are assumed constant, and they are given in Table 1 (Golneshan and Lahonian, 2011; Hergt et al., 1998; Kappiyoor et al., 2010; Nicholson, 2001).

All above parameters are average on the whole cancerous brain tissue. The most researchers in the biomechanics, consider boundary conditions for various tissues as zero gradient (Hergt et al., 2006). Therefore initial and boundary conditions for Eq. (1) define as below:

$$\frac{\partial C}{\partial x} = 0 \quad at\ x = 0 \tag{5}$$

$$\frac{\partial C}{\partial x} = 0 \quad at\ x = L \tag{6}$$

$$\frac{\partial C}{\partial y} = 0 \quad at\ y = 0 \tag{7}$$

$$\frac{\partial C}{\partial y} = 0 \quad at\ y = L \tag{8}$$

$$C(x, y, t) = 0 \quad for\ t = 0 \tag{9}$$

Boundary and initial conditions for Eq. (3) define as:

$$\frac{\partial T}{\partial x} = 0 \quad at\ x = 0 \tag{10}$$

$$\frac{\partial T}{\partial x} = 0 \quad at\ x = L \tag{11}$$

$$\frac{\partial T}{\partial y} = 0 \quad at\ y = 0 \tag{12}$$

$$\frac{\partial T}{\partial y} = 0 \quad at\ y = L \tag{13}$$

$$T(x, y, t) = 37^{\circ}C\ for\ t = 0 \tag{14}$$

Firstly, the initial location of injection points and SLP are,randomly, assumed, then by using inverse method, the new values are calculated, and this process continues until the convergence of the method. The details of the mathematical process are as follows.

3. Mathematical methods

Injection points of nanoparticles are playing an important role in the effectiveness of MFH. As a matter of fact, imprecise injection points impede the uniform distribution of nanoparticles which ultimately lead to non-uniform temperature distribution. In order to achieve a uniform distribution of nanoparticles, a mathematical model to obtain precise injection points is required. The mentioned model have to be accurate enough and at the same time simple to be used in complex problems.

3.1. Inverse method

Classical solving methods are unable to obtain any unknown quantities in each differential equation without boundary and initial conditions. Inverse methods by minimizing an objective function with some iterative techniques can estimate the parameters and also the accurate amount of unknown quantities. The objective function, S, that provides minimum variance estimates, is the ordinary least squares norm defined as (Ozisik et al., 2002):

$$S(P) = [Y - W(P)]^T [Y - W(P)] \tag{15}$$

where Y and W are the vectors containing the desired and the calculated quantities, respectively, P is the vector of the unknown

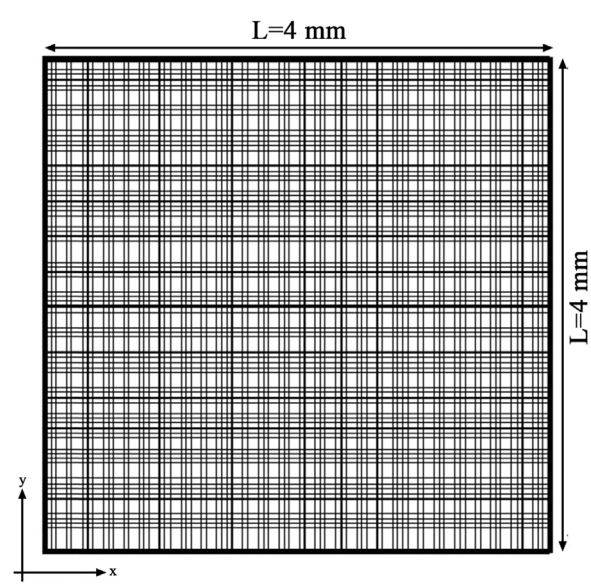

Fig. 1. Physical domain of the cancerous tissue and its mesh distribution.

Table 1
Thermophysical and physical properties of the brain cancerous tissue.

Parameter	Value	Parameter	Value
ρ (kg/m^3)	1196	T_b (°C)	37
C_p (J/kgK)	2279	q_m (W/m^3)	1190
k (W/mK)	0.58	D^* (m^2/s)	5×10^{-11}
ω_b (m^3/m^{3}tissue)	0.009	α	0.1
ρ_b (kg/m^3)	1060	V (cm^3)	0.2
C_{pb} (J/kgK)	3860	Q (μl/min)	10

parameters and the superscript T indicates the transpose of the vector. In the recent year, variety of techniques have been presented to minimize the objective function of different inverse problems. In this study, conjugate gradient technique which is a straightforward and powerful iterative technique for solving linear and nonlinear inverse problems is used to obtain the precise injection points.

3.2. Conjugate gradient technique

Minimization of the objective function is achieved by the following iterative procedure (Ozisik et al., 2002):

$$P^{k+1} = P^k - \beta^k d^k \tag{16}$$

where β^k is the search step size, d^k is the direction of the descent and the superscript k is the number of iterations. The direction of the descent is described as follows (Ozisik et al., 2002):

$$d^k = \nabla S(P^k) + \gamma^k d^{k-1} \tag{17}$$

where $\nabla S(P^k)$ is the gradient direction of the iteration and γ^k is the conjugation coefficient which is given as (Ozisik et al., 2002):

$$\gamma^k = \frac{\sum_{j=1}^{N} \{[\nabla S(P^k)]_j [\nabla S(P^k) - \nabla S(P^{k-1})]_j\}}{\sum_{j=1}^{N} [\nabla S(P^{k-1})]_j^2} \quad k = 1, 2, \ldots, n \tag{18}$$

with $\gamma^k = 0$ for $k = 0$

In above equation, $[\nabla S(P^k)]_j$ is the jth component of the gradient direction at k^{th} iteration. The gradient direction can be obtained from the following equation (Ozisik et al., 2002):

$$\nabla S(P^k) = -2(J^k)^T [Y - W(P^k)] \tag{19}$$

where J^k is the sensitivity matrix which is expressed as follow (Ozisik et al., 2002):

$$J^k = \left[\frac{\partial W(P^k)}{\partial P}\right]^T \tag{20}$$

Therefore, the jth component of the gradient direction, in explicit form, can be obtained as below (Ozisik et al., 2002):

$$[\nabla S(P^k)]_j = -2 \sum_{j=1}^{n} \frac{\partial W_i^k}{\partial P_j} [Y_i - W_i(P^k)] j = 1, 2, \ldots, n \tag{21}$$

The search step size β^k is obtained by minimizing the function $S(P^{k+1})$ with respect to β^k (Ozisik et al., 2002):

$$\beta^k = \frac{\sum_{i=1}^{N} \left\{\left(\frac{\partial W_i}{\partial P^k}\right)^T d^k\right\} [W_i(P^k) - Y_i]}{\sum_{i=1}^{N} \left\{\left(\frac{\partial W_i}{\partial P^k}\right)^T d^k\right\}^2} \tag{22}$$

The iterative procedure would be stopped if the maximum change in gradient direction $S(P^k)$ at any point be less than ε, which is considered as 10^{-6} in the present study.

3.3. Solution procedure

In this study, governing equations of a cancerous brain tissue in a 2D square domain were solved with the inverse method. It should be noted that in the present approach, the conjugate gradient technique is used to obtain the nanoparticle concentration and temperature.

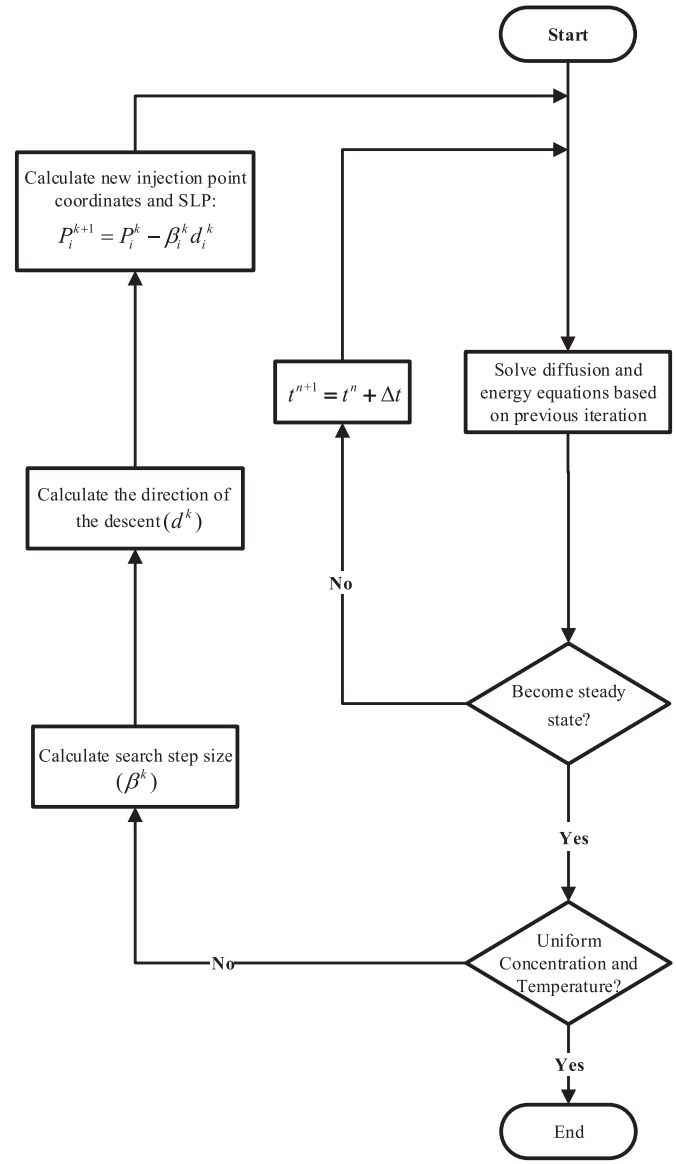

Fig. 2. Flowchart of the inverse technique using the conjugate gradient method applied in this study. The converge criteria in this study are uniform concentration and temperature (the desired temperature is 43 °C).

Computations of energy and mass diffusion equations are performed by the following flowchart:

- Initialize injection point coordinates with random input.

➢ Compute nanoparticle concentration and temperature fields for each time step based on the mass diffusion and energy equations, respectively.
➢ Repeat the iterative process until the steady-state criterion is obtained.

- Compute the new injection point coordinate based on the conjugate gradient technique.
- Repeat the iterative process until convergence is achieved for uniform nanoparticle concentrations and temperatures.

These levels are shown in the following flowchart that is drawn in

the Fig. 2.

3.4. Grid sensitivity and model verification

Grid independence of the results has been established for the thermophysical and physical properties of the tissue which are given in Table 1. Fig. 3 displays the variation of the magnitude of the tissue temperature and nanoparticles concentration on the horizontal mid-plane $\left(\frac{y}{L} = 0.5\right)$ for four grids 25 × 25, 50 × 50, 100 × 100, 200 × 200. No significant change in the results are observed for two grids of 100 × 100 and 200 × 200. Hence the suitable grid for this problem is considered as 100 × 100.

To validate the present numerical model, the variation of concentrations are compared with experimental ones obtained by Crank (Crank, 1975). The concentration of injected liquid in the tissue 20 min after injection is compared with those given in the experimental study (Crank, 1975) as shown in Fig. 4. For this validation process, the results are presented for the injection volume of $V = 0.2\,\text{cm}^3$, the injection rate of $Q = 30\,\mu\text{l/min}$, and the porosity of $\alpha = 0.1$. An excellent agreement is found between the present results and experimental ones reported in the mentioned reference. It should be noted that the maximum error in the concentration of injected liquid does not exceed 5%.

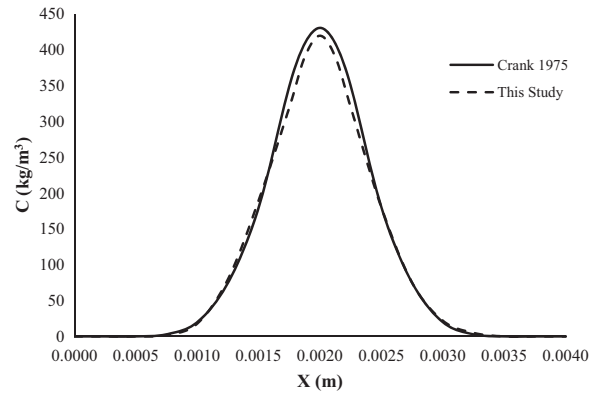

Fig. 4. Comparison of the numerical results of the present work with the experimental results of (Crank, 1975).

4. Results and discussion

In the present study, precise injection points and optimum amount of SLP for three types of multi-site injections are investigated through inverse method proposed in Section 3. In this part, results of numerical simulations are presented and analyzed.

4.1. Coordinate of precise injection points

Estimation of the precise injection points, in fact, is a determination of x and y positions of the injection points which produce the best possible uniform nanoparticle distribution. The process of finding precise injection points and optimum amount of SLP happens together, but for clarifying, precise injection points is described in this section and optimum amount of SLP is described in the following section. Fig. 5 shows the points estimated by the inverse method, by using conjugate gradient technique in the physical domain for three types of multi-site injection. The locus of estimated and precise injection points are displayed by dot, dash, and solid lines, respectively. Initial guess is absolutely fortuitous, as the effect of initial guess on the convergence time is not noticeable. Inverse method at each iteration use the error between the measured and desired results and calculates new coordinates. The iterative procedure is stopped, when convergence criteria are achieved which indicate that the best nanoparticles locations are obtained. The iteration process becomes more complex and difficult by increasing the number of injections. As can be seen in Fig. 5, estimation of the precise injection points for three-point injection, four-point injection, and five-point injection take 17, 25 and 36 iterations, respectively. The locus of estimated points in five-point injection has also changed more through the iteration process compared to other multi-site injection. The optimum coordinates of three-point injection are ((1.32,1.40), (2.00,2.00), (3.00,2.60)), and these coordinates for four-point injection are ((1.04,2.76), (2.80,2.76), (1.00,1.00), (2.84,1.00)) while for five-point injection these are ((0.80,3.24); (3.20,3.24); (2.00,2.00); (0.80,0.84); (3.32,0.84)), all dimensions are in mm.

4.2. Optimum amount SLP

The precise coordinates of the injection points were found in Section 4.1. Optimum amount of SLP for injection points is our next step. Although this process happened with the finding precise injection point at the same time, the detail of finding optimum amount of SLP is described here. The steady state temperature and concentration distributions in the tissue for certain iterations are plotted in Fig. 6, Fig. 7, and Fig. 8, for different multi-site injections. The optimum amount of SLP producing the uniform temperature distribution is obtained based on the iterative procedure. The coordinate of injection points which result in the uniform temperature would be changed during the iterations, in order to find the precise injection points. It is worth remembering that the uniform temperature distribution is largely dependent on SLP. As a matter of fact, there is a direct relationship between SLP and the tissue temperature distribution.

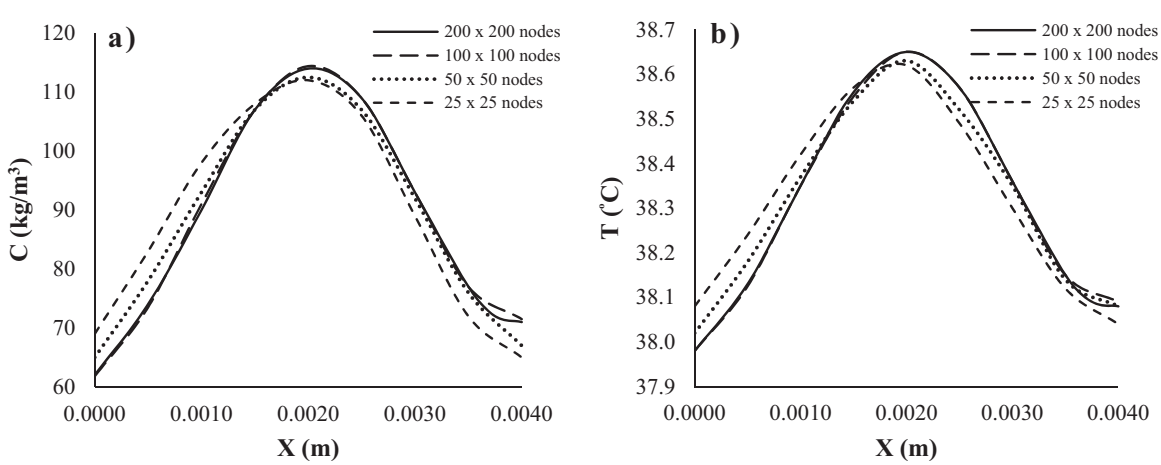

Fig. 3. Grid independence study for a) nanoparticle concentration b) temperature distribution.

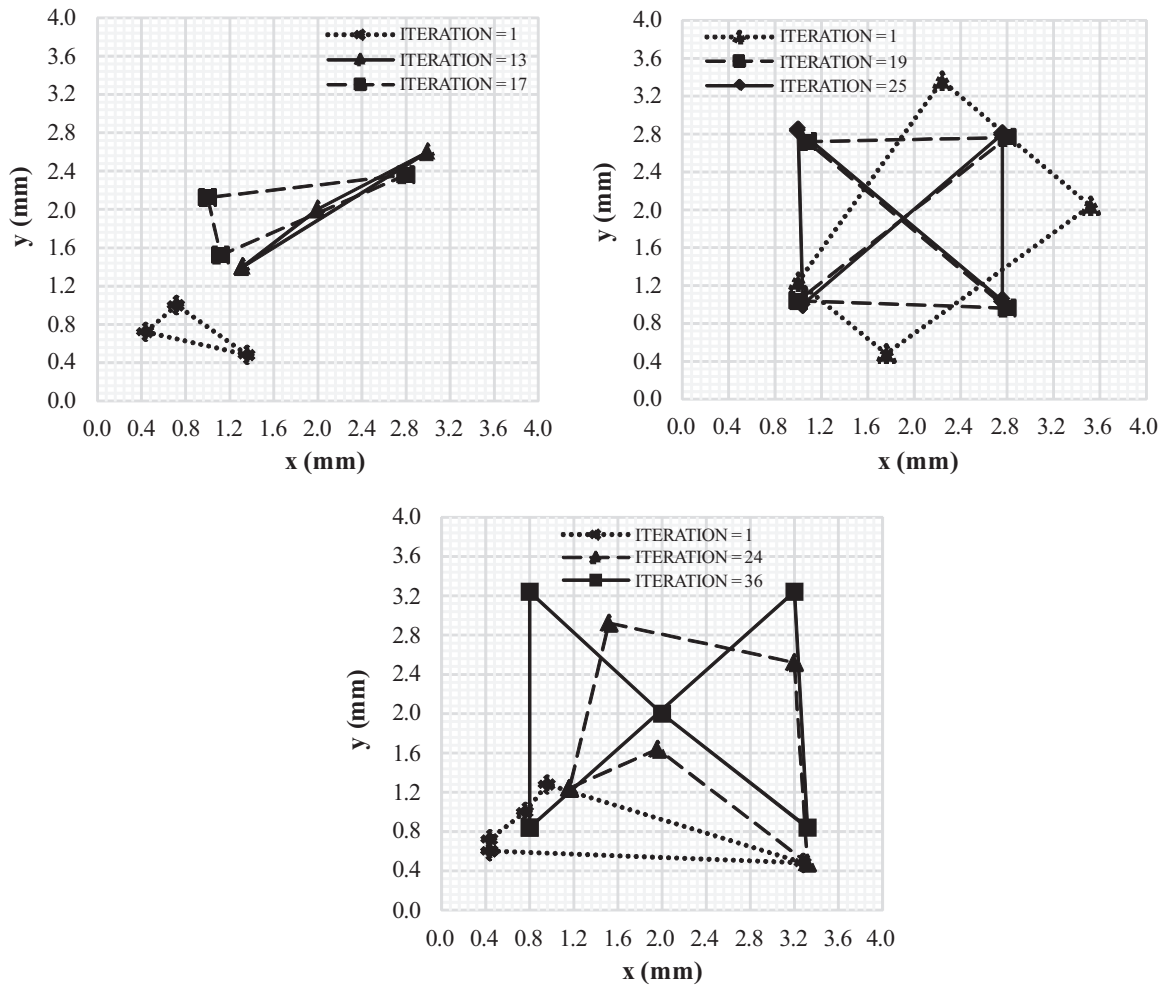

Fig. 5. Problem solving process by the inverse conjugate gradient technique iterations for estimating the precise injection points over the cancerous domain for a) three-point injection b) four-point injection c) five-point injection.

4.2.1. *Three-point injection*

Fig. 6 shows the effect of the estimated SLP during the iteration for three-point injection on the distribution of nanoparticle concentration and temperature in the computational domain. As can be seen in this figure, the amount of SLP has changed through the iterative procedure. The locus of estimated points has also changed during the iterative procedure. The optimum amount of SLP is 521 W/g which is obtained after 17 iterations. However, the optimum SLP cannot provide the desired temperature distribution as it is shown the figure.

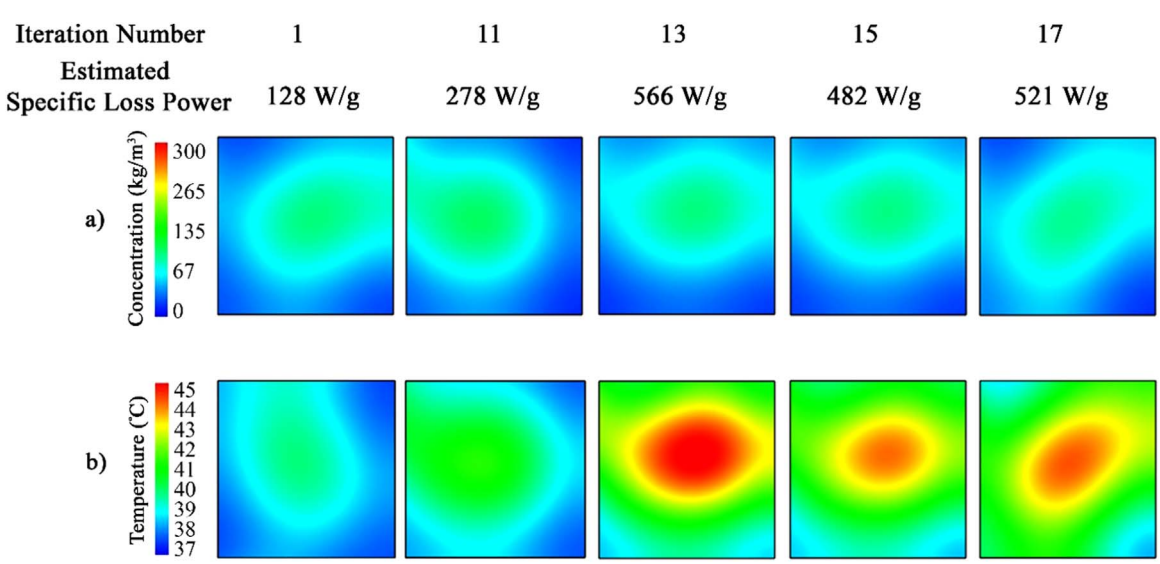

Fig. 6. The effect of the estimated SLP on the nanoparticle concentration and temperature distribution in different iterations for three-point injection.

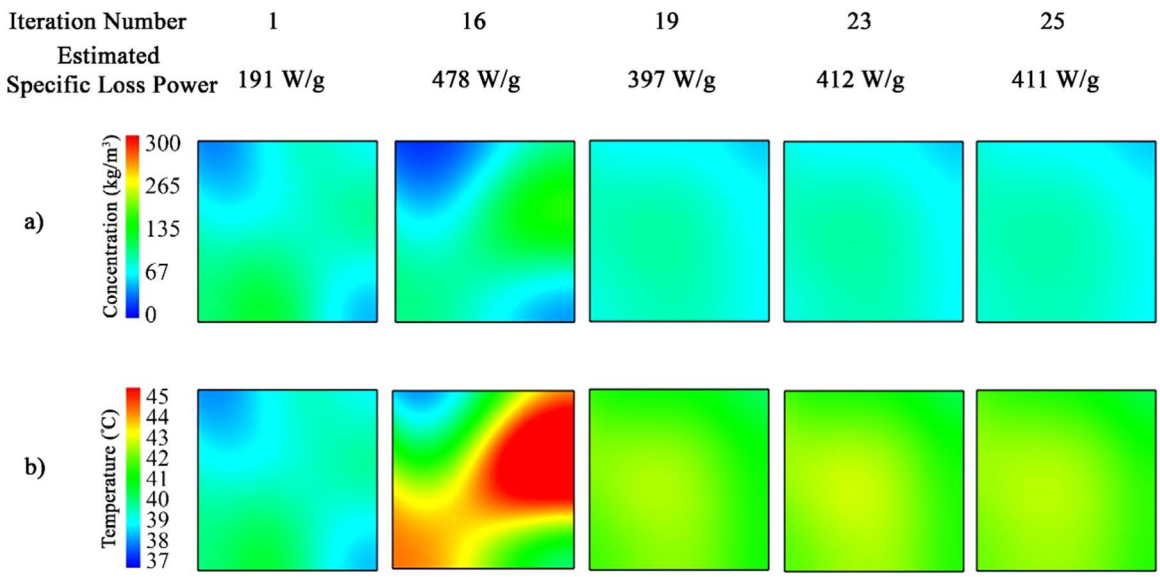

Fig. 7. The effect of the estimated SLP on the nanoparticle concentration and temperature distribution in different iterations for four-point injection.

4.2.2. Four-point injection

The estimated SLP for four-point injection is shown in Fig. 7. According to the Fig. 7, the 411 W/g is the optimum SLP for four-point injection. The amount of the optimum SLP for four-point injection which is achieved after 25 iterations is smaller than that of three-point injection. Although the temperature distribution is uniform, the referred SLP cannot provide the desired temperature distribution (43 °C) in the domain. Therefore, additional injected point is necessary.

4.2.3. Five-point injection

Considering five-point injection, the estimated SLP is shown in Fig. 8. According to the Fig. 8, the optimum SLP for this site injection is 420 W/g. The optimum SLP for five-point injection is achieved after 36 iterations which indicates that the iteration process becomes more complex by increasing the number of injections. Therefore, the number of iterations in three-point injection is smaller than that of five-point injection. The optimum amount of SLP in the five-point injection not only supplies uniform distribution but also provides the desired temperature distribution in the domain.

4.3. Nanoparticle concentration and temperature distribution

After the injection of nanoparticles in the tissue based on precise injection points, the nanoparticles are given about three hours to become steady when the magnetic field is applied to generate heat in the tissue and increase its temperature. For better understanding the process, the coordinates of injection points, nanoparticle concentration over time, and the ultimate temperature contour for different types of multi-site injections are displayed in Fig. 9, Fig. 10, and Fig. 11.

4.3.1. Three-point injection

The coordinate of injection points in the three-point injection is displayed in Fig. 9a. According to this figure, three points which are arranged in diagonal lines can make the most uniform nanoparticle concentration compared to the other three-point injection arrangement. Fig. 9b shows the distribution of nanoparticle concentrations in the computational domain over time. It can be seen that the nanoparticle concentration is relatively uniform about 12,200 s after the beginning of injection. The steady temperature distribution is shown in Fig. 9c. The nanoparticle concentration reaches locally the objective

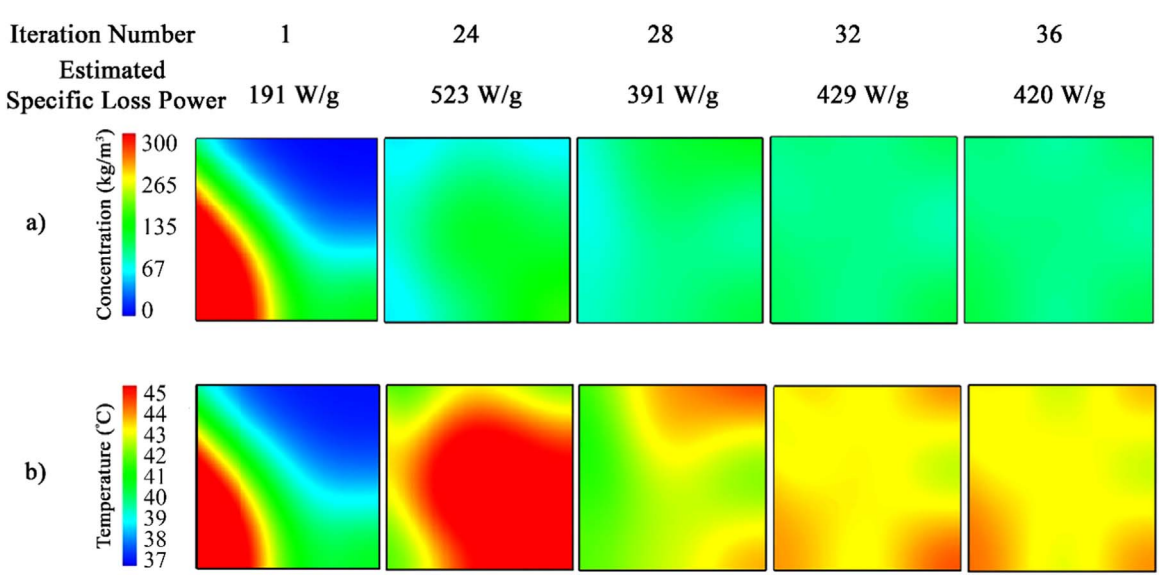

Fig. 8. The effect of the estimated SLP on the nanoparticle concentration and temperature distribution in different iterations for five-point injection.

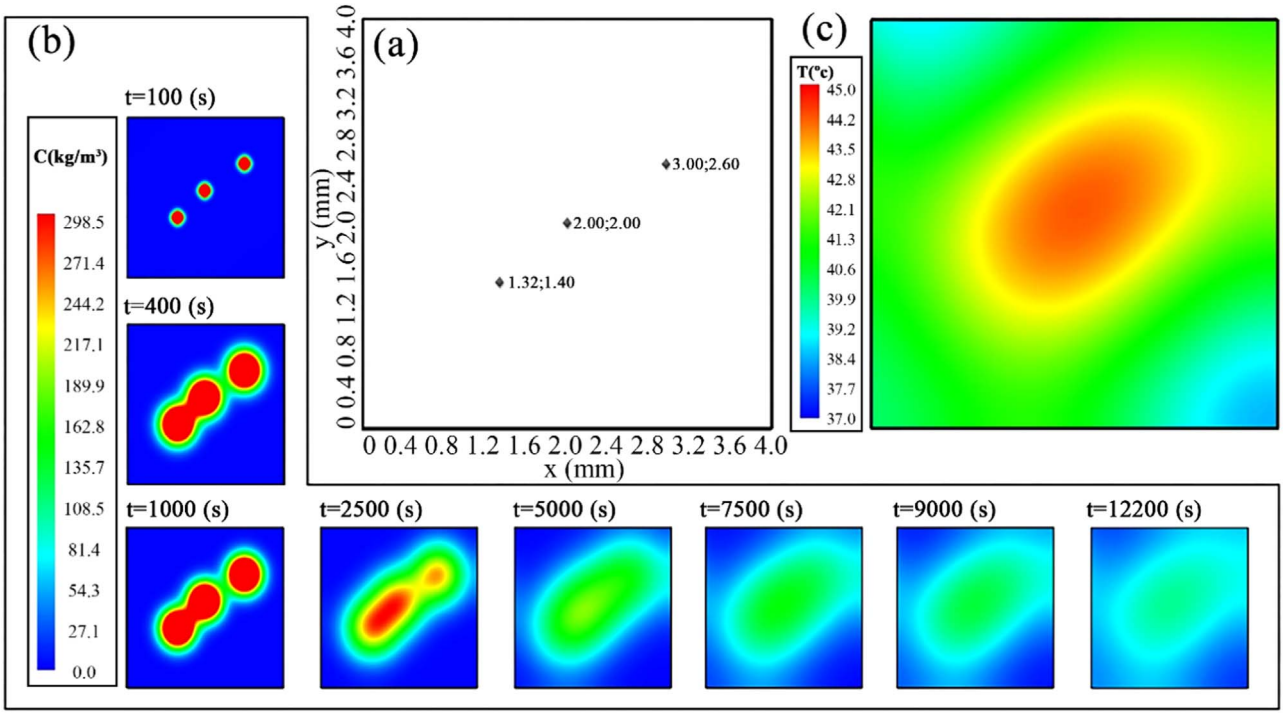

Fig. 9. Different parts of the nanoparticle concentration and the temperature distribution for three-point injection a) estimated sites of injection points b) distribution of the nanoparticle concentration over time c) steady state temperature distribution,12,200 s after the ferrofluid injection.

temperature (43 °C). In other words, this form of injection cannot provide the desired temperature distribution which results in tumor regression.

4.3.2. Four-point injection

Fig. 10 shows the results for four-point injection. The locus of injection points in the four-point injection is a square concentric with the physical domain as it is shown in Fig. 10a. The way that the nanoparticle concentration of the each point is changed over the time is shown in Fig. 10b. After 9000 s, the uniform nanoparticle concentration distribution occurred, approximately. Fig. 10c shows the steady temperature distribution for four-point injection. As contrasting to three-point injection, the four-point injection can provide a complete uniform nanoparticle concentration. This uniform nanoparticle concentration

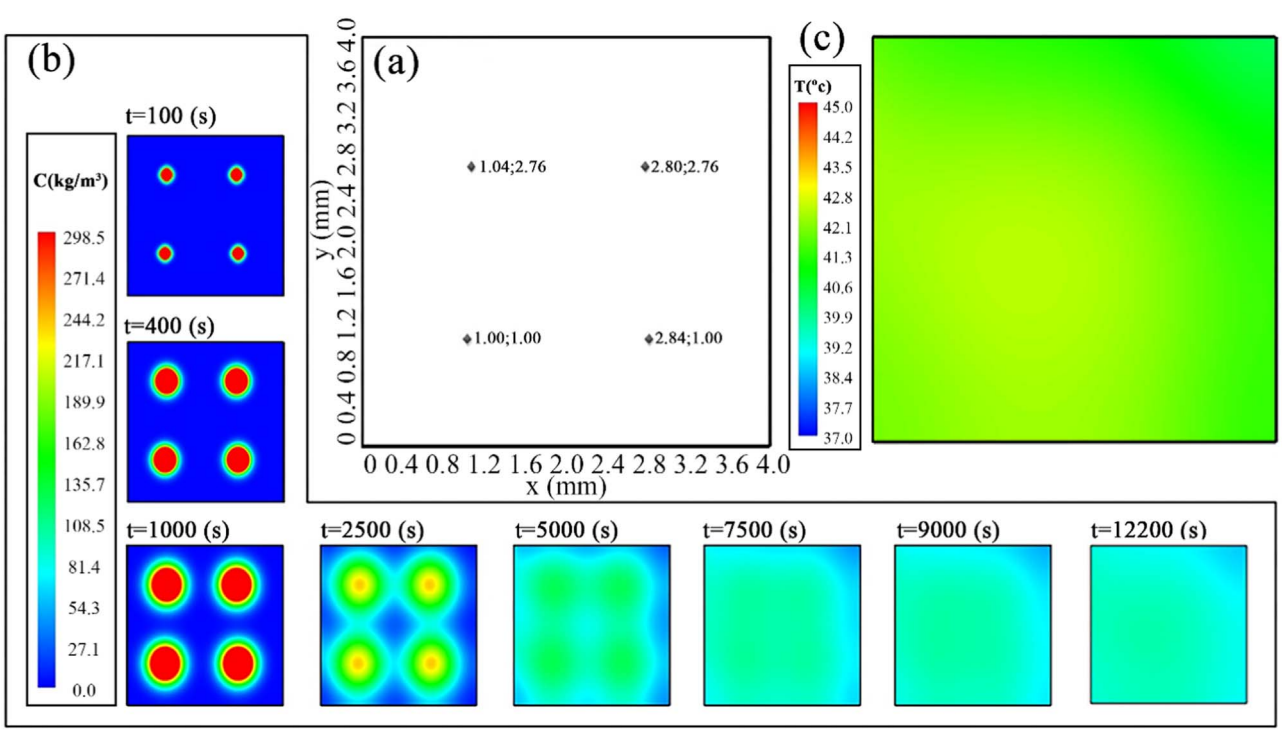

Fig. 10. Different parts of the nanoparticle concentration and the temperature distribution for four-point injection a) estimated sites of injection points b) distribution of the nanoparticle concentration over time c) steady state temperature distribution,12,200 s after the ferrofluid injection.

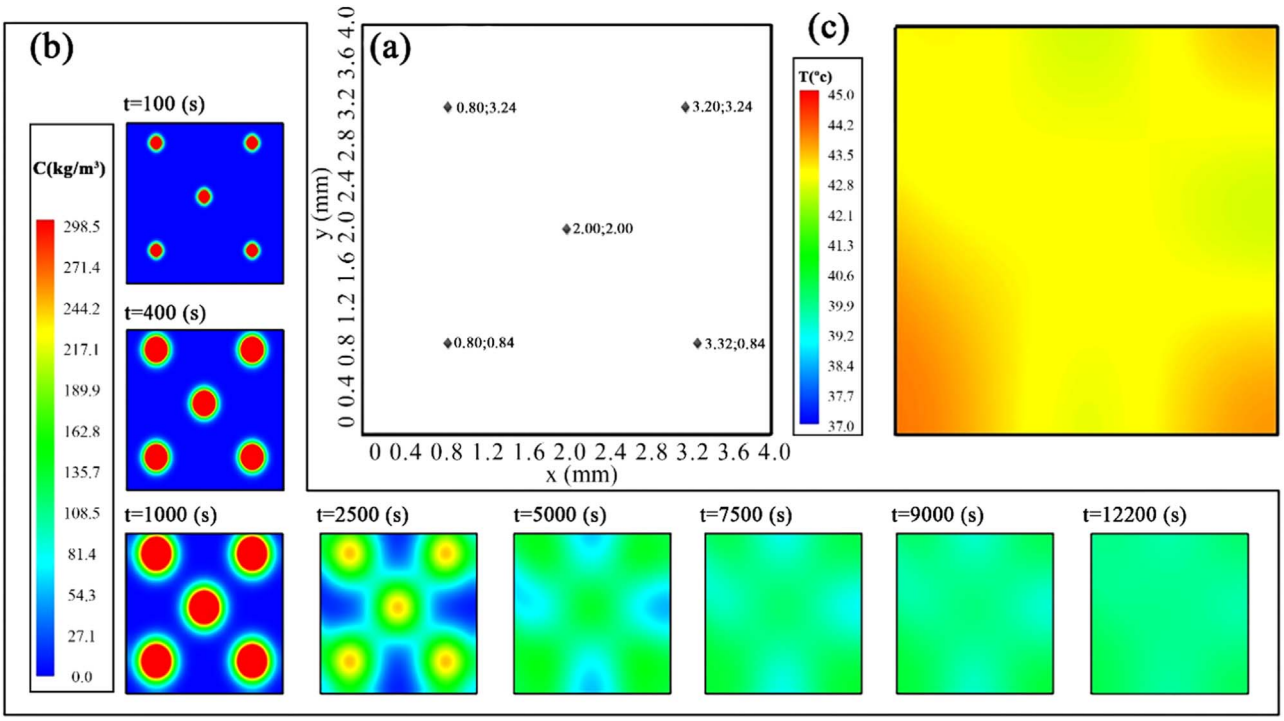

Fig. 11. Different parts of the nanoparticle concentration and the temperature distribution for five-point injection a) estimated sites of injection points b) distribution of the nanoparticle concentration over time c) steady state temperature distribution,12,200 s after the ferrofluid injection.

results in a uniform temperature distribution. However, the nanoparticle concentration is not able to provide the objective temperature (43 °C) in the domain. Although it can raise by increasing the amount of injection, uniform nanoparticle concentration with the optimum amount of injection is desired. Additionally, the tumor cells in the regions with the temperature less than 43 °C may reproduce and change its shape into the more complex one. Therefore, the four-point injection cannot be regarded as a suitable site injection for tumor regression.

4.3.3. Five-point injection

The results of the injection for five points are shown in Fig. 11. As can be seen in Fig. 11a, the location of injection points in the five-point injection is a quincunx whose center is the same as the square domain. The nanoparticle concentration over the time domain is shown in the Fig. 11b. It can be seen that the nanoparticle concentration is completely uniform after 12,200 s Fig. 11c demonstrates the steady temperature distribution in the physical domain. The nanoparticle concentration has provided the objective temperature (43 °C) in the entire domain which can provide the required circumstances for tumor cells regression.

As a result, the Optimum SLP for three-point injection, four-point injection, and five-point injection is 521 W/g, 411 W/g, and 420 W/g, respectively and only five-point injection can provide hyperthermia with required temperature distribution. Therefore, the five-point injection can be considered as a suitable injection for MFH.

5. Conclusion

Uniform 43 °C temperature distribution at the cancerous tissue is vital for effective MFH. This temperature distribution is only achieved by uniform nanoparticle concentration distribution and the optimum amount of SLP which can be acquired by complex inverse methods. For this purpose, the conjugate gradient technique was used to obtain both precise injection points and the optimum amount of SLP in a 2D square cancerous brain tissue. The results showed that opposed to three-point injection and four-point injection failing to meet the demands, five-point injection gains a uniform temperature distribution in the coordinates of ((0.80,3.24), (0.80,0.84), (2.00,2.00), (3.20,3.24), (3.32,0.84)) (all dimensions are in mm). Therefore, the temperature distribution in steady-state demonstrates that in the physical domain, with five-point injection and their relative optimum coordinates, as well as optimum amount of SLP which is 420 W/g, the desired condition for a complete tomour regression occurs.

Acknowledgements

This research did not receive any specific grant from funding agencies in the public, commercial, or not-for-profit sectors.

References

Atsumi, T., Jeyadevan, B., Sato, Y., Tohji, K., 2006. Fundamental studies of hyperthermia using magnetic particles as thermo-seeds 1: development of magnetic particles suitable for hyperthermia. J.-Magn. Soc. Jpn. 30, 555.
Baghban, M., Ayani, M., 2015. Source term prediction in a multilayer tissue during hyperthermia. J. Therm. Biol. 52, 187–191.
Baghban, M., Ayani, M.B., 2017. Estimation of surface heat flux in a one-dimensional hyperbolic bio-heat conduction problem with temperature-dependent properties during thermal therapy. J. Braz. Soc. Mech. Sci. Eng. 39, 1479–1489.
Brusentsov, N.A., Nikitin, L.V., Brusentsova, T.N., Kuznetsov, A.A., Bayburtskiy, F.S., Shumakov, L.I., Jurchenko, N.Y., 2002. Magnetic fluid hyperthermia of the mouse experimental tumor. J. Magn. Magn. Mater. 252, 378–380.
Crank, J., 1975. The Mathematics of Diffusion, 2d ed. Clarendon Press.
Davson, H., 1993. An Introduction to the Blood-brain Barrier. CRC PressI Llc.
Deatsch, A.E., Evans, B.A., 2014. Heating efficiency in magnetic nanoparticle hyperthermia. J. Magn. Magn. Mater. 354, 163–172.
Deger, S., Böhmer, D., Rüter, A., Roigas, J., Budach, V., Loening, S., 2003. Interstitial hyperthermia using self-regulating thermoseeds combined with conformal radiation therapy. Eur. Urol. Suppl. 2, 136.
Golneshan, A.A., Lahonian, M., 2011. Diffusion of magnetic nanoparticles in a multi-site injection process within a biological tissue during magnetic fluid hyperthermia using lattice Boltzmann method. Mech. Res. Commun. 38, 425–430.
Habash, R.W., Bansal, R., Krewski, D., Alhafid, H.T., 2006. Thermal therapy, part 1: an introduction to thermal therapy. Crit. Rev.™ Biomed. Eng. 34.
Hergt, R., Andra, W., d'Ambly, C.G., Hilger, I., Kaiser, W.A., Richter, U., Schmidt, H.-G., 1998. Physical limits of hyperthermia using magnetite fine particles. Magn. IEEE Trans. 34, 3745–3754.
Hergt, R., Dutz, S., Müller, R., Zeisberger, M., 2006. Magnetic particle hyperthermia: nanoparticle magnetism and materials development for cancer therapy. J. Phys.:

Condens. Matter 18, S2919.
Jain, R.K., Tong, R.T., Munn, L.L., 2007. Effect of vascular normalization by anti-angiogenic therapy on interstitial hypertension, peritumor edema, and lymphatic metastasis: insights from a mathematical model. Cancer Res. 67, 2729–2735.
Jalali, A., Ayani, M.-B., Baghban, M., 2014. Simultaneous estimation of controllable parameters in a living tissue during thermal therapy. J. Therm. Biol. 45, 37–42.
Johannsen, M., Jordan, A., Scholz, R., Koch, M., Lein, M., Deger, S., Roigas, J., Jung, K., Loening, S., 2004. Evaluation of magnetic fluid hyperthermia in a standard rat model of prostate cancer. J. Endourol. 18, 495–500.
Jordan, A., Scholz, R., Wust, P., Fähling, H., Felix, R., 1999. Magnetic fluid hyperthermia (MFH): cancer treatment with AC magnetic field induced excitation of biocompatible superparamagnetic nanoparticles. J. Magn. Magn. Mater. 201, 413–419.
Kappiyoor, R., Liangruksa, M., Ganguly, R., Puri, I.K., 2010. The effects of magnetic nanoparticle properties on magnetic fluid hyperthermia. J. Appl. Phys. 108, 094702.
Katz, E., Willner, I., 2004. Integrated nanoparticle–biomolecule hybrid systems: synthesis, properties, and applications. Angew. Chem. Int. Ed. 43, 6042–6108.
Laurent, S., Dutz, S., Häfeli, U.O., Mahmoudi, M., 2011. Magnetic fluid hyperthermia: focus on superparamagnetic iron oxide nanoparticles. Adv. Colloid Interface Sci. 166, 8–23.
Liu, X.L., Fan, H.M., Yi, J.B., Yang, Y., Choo, E.S.G., Xue, J.M., Di Fan, D., Ding, J., 2012. Optimization of surface coating on Fe_3O_4 nanoparticles for high performance magnetic hyperthermia agents. J. Mater. Chem. 22, 8235–8244.
Mohajer, M., Ayani, M.B., Tabrizi, H.B., 2016. Numerical study of non-Fourier heat conduction in a biolayer spherical living tissue during hyperthermia. J. Therm. Biol. 62, 181–188.
Nicholson, C., 2001. Diffusion and related transport mechanisms in brain tissue. Rep. Prog. Phys. 64, 815.
Ozisik, M., Orlande, H., Kassab, A., 2002. Inverse heat transfer: fundamentals and applications. Appl. Mech. Rev. 55, B18.
Park, B.-H., Koo, B.S., Kim, Y.K., Kim, M.K., 2002. The induction of hyperthermia in rabbit liver by means of duplex stainless steel thermoseeds. Korean J. Radiol. 3, 98–104.
Pennes, H.H., 1948. Analysis of tissue and arterial blood temperatures in the resting human forearm. J. Appl. Physiol. 1, 93–122.
Salloum, M., Ma, R., Zhu, L., 2009. Enhancement in treatment planning for magnetic nanoparticle hyperthermia: optimization of the heat absorption pattern. Int. J. Hyperth. 25, 309–321.
Smolkova, I.S., Kazantseva, N.E., Babayan, V., Smolka, P., Parmar, H., Vilcakova, J., Schneeweiss, O., Pizurova, N., 2015. Alternating magnetic field energy absorption in the dispersion of iron oxide nanoparticles in a viscous medium. J. Magn. Magn. Mater. 374, 508–515.
Soltani, M., Chen, P., 2011. Numerical modeling of fluid flow in solid tumors. PLoS One 6, e20344.
Tartaj, P., Serna, C.J., 2003. Synthesis of monodisperse superparamagnetic Fe/silica nanospherical composites. J. Am. Chem. Soc. 125, 15754–15755.
Vallejo-Fernandez, G., O'Grady, K., 2013. Effect of the distribution of anisotropy constants on hysteresis losses for magnetic hyperthermia applications. Appl. Phys. Lett. 103, 142417.